Paper
Int'l J. of Aeronautical & Space Sci. 17(3), 358–365 (2016)
DOI: http://dx.doi.org/10.5139/IJASS.2016.17.3.358

# Analytical Performance Evaluation of Superdetonative Mode Ram Accelerator; Considering Influence of Aluminum Vapor

**Kunmin Sung* and In-Seuck Jeung****

*Institute of Advanced Aerospace Technology, Department of Mechanical and Aerospace Engineering, Seoul National University, Seoul 08826, Republic of Korea*

## Abstract

In this study, one-dimensional analysis under the assumption of an inviscid flow was conducted for the experiment initiated by the French-German Research Institute of Saint-Louis (ISL) in order to investigate the energy effect of aluminum combustion. Previous theoretical analysis based on the assumptions of isentropic compression and a constant specific heat derived by ISL claimed that the experiment was not affected by the heat of aluminum combustion. However, rigorous analysis in present investigation that considered the average properties behind the shock wave compression and temperature-dependent specific heat showed that the S225 experiment was partially affected by the aluminum combustion. The increase in heat due to aluminum combustion was estimated from the rigorous analysis.

**Key words:** Ram Accelerator, Superdetonative Mode, Aluminum Combustion

## 1. Introduction

The ram accelerator is a device used to accelerate projectiles with synchronized combustion through a tube filled with a premixed combustible gas mixture [1]. A projectile is accelerated continuously through a ram tube; thus, a high final speed can be obtained with a long ram tube. Ram accelerators can be utilized as hypervelocity launchers or direct launchers for low Earth orbits [2].

The operation mode of the ram accelerator depends on the speed of the projectile and Chapman-Jouguet (C-J) detonation speed of the combustible gas mixture [1]. The projectile flies slower than the C-J detonation speed in subdetonative mode; the maximum speed is limited by the C-J detonation speed. In this mode, the combustion wave is typically stabilized by thermal choking at the base of the projectile (Fig. 1a). Since the first experiment conducted at Washington University [1], a number of experimental studies and numerical simulations have been conducted for this operation mode. The maximum speed achieved was approximately 2700 m/s. The projectile flies faster than the C-J detonation speed in superdetonative mode. An ultimate projectile speed that is above the C-J detonation

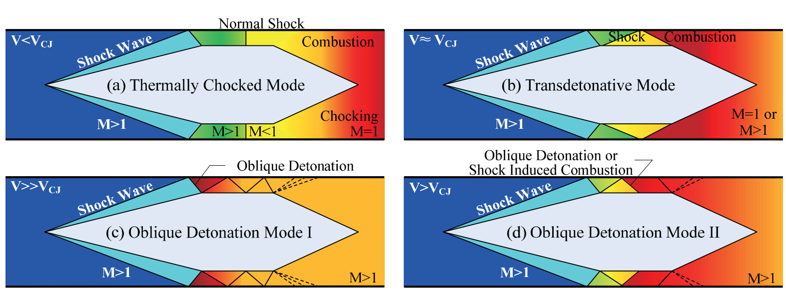


Fig. 1. Operating mode of ram accelerator



* Ph. D. Student
** Professor, Corresponding author : enjis@snu.ac.kr

Received: June 13, 2016 Revised: July 9, 2016 Accepted: August 19, 2016

speed can be achieved in this mode. The detonation wave can be stabilized at the reflecting point on the tube wall at very high Mach numbers (Fig. 1c), or can be stabilized by shock wave induced combustion when the projectile is not fast enough to directly initiate detonation (Fig. 1d).

The French-German Research Institute of Saint-Louis (ISL) developed a rail tube version of a ram accelerator facility named RAMAC 30 version II that directly launches projectiles at superdetonative speed [3]. Fig. 2 shows a schematic of RAMAC 30 version II, and table 1 shows the setup of experiment shot 225. Although the initial launching speed of the projectile was only 1800 m/s, superdetonative launch was made possible by using an $H_2/O_2/CO_2$ mixture having a low C-J detonation wave speed. Successful acceleration was observed in the experiment using the aluminum projectile, whereas deceleration was observed for the steel projectile. The aluminum projectile showed significant ablation [3, 4]. Thus, there were less understood issues that the ablation of a projectile might be related to the ignition and combustion of a gas mixture. The mechanism of ignition and propulsion has not yet been clarified.

Previously, ISL conducted a theoretical study assuming a constant specific heat and isentropic compression and showed that the heat of the aluminum did not affect the acceleration [5]. However, rigorous analysis may be necessary to investigate the effect of aluminum combustion. In the present study, theoretical analysis was conducted under a rigorous approach to understand the experimental results of ISL RAMAC30 II. Simplified analysis was conducted for comparison with the rigorous analysis.

## 2. Theoretical Methods: solution procedures of quasi one-dimensional system

The ram projectile flies in the supersonic flow region, and most of the drag is caused by pressure drag. The inflow conditions are not disturbed by the ram projectile. Therefore, steady-state quasi one-dimensional analysis under the assumption of an inviscid flow can be applied to superdetonative mode ram accelerators. The conservation laws for mass, momentum, and energy and the equation of state are as follows:

Continuum Equation:

$$\rho_i u_i A_i = \rho_e u_e A_e \tag{1}$$

Momentum Equation:

$$\left(P_i + \rho_i u_i^2\right) A_i + F = \left(P_e + \rho_e u_e^2\right) A_e \tag{2}$$

Energy Equation:

$$h_i + \frac{1}{2}u_i^2 = h_e + \frac{1}{2}u_e^2 \tag{3}$$

Equation of State:

$$P = \rho RT \text{ or } \rho = \frac{P}{RT} \tag{4}$$

Subscript $i$ refers to the inflow state of the process, and subscript $e$ refers to the outflow state of the process. In order to determine the state of flow, pressure $P$, density $\rho$, temperature $T$, and speed $u$ are required; enthalpy $h$ is a function of the temperature for ideal gases. If the inflow state is known, the four unknowns ($P_e, \rho_e, T_e, u_e$) can be determined from four equations (Eqs. (1)–(4)). Density $\rho$ can be canceled in Eq. (2) with Eq. (4).

$$\left(P_i + \frac{P_i}{R_i T_i}u_i^2\right)A_i + F = \left(P_e + \frac{P_e}{R_e T_e}u_e^2\right)A_e$$

$$\left(1 + \frac{u_i^2}{R_i T_i}\right) + \tilde{F} = \left(1 + \frac{u_e^2}{R_e T_e}\right)\frac{P_e A_e}{P_i A_i}$$

Here, $\tilde{F} = F/P_i A_i$ is a non-dimensional force that can be either thrust or drag. Using the Mach number $M$ instead of the speed $u$ is more efficient for supersonic flows. The speed can be defined according to the Mach number and speed of sound:

$$u = Ma = M\sqrt{\gamma RT} \tag{5}$$

Using Eq. (5), Mach number $M$ can replace speed $u$.

$$\left(1 + \gamma_i M_i^2\right) + \tilde{F} = \left(1 + \gamma_e M_e^2\right)\frac{P_e A_e}{P_i A_i} \tag{6}$$

The pressure ratio can be derived from Eq. (6):

$$\frac{P_e}{P_i} = \frac{A_i}{A_e}\frac{\left(1 + \gamma_i M_i^2\right) + \tilde{F}}{1 + \gamma_e M_e^2} \tag{7}$$

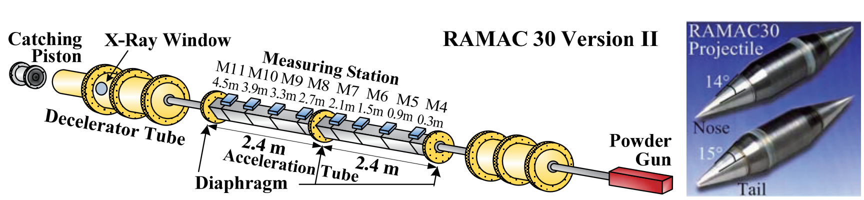


Fig. 2. Schematic of RAMAC 30 II and projectile

If the Mach number and $\tilde{F}$ are known at two states, the pressure ratio can be obtained from Eq. (7). Density $\rho$ can be canceled in Eq. (1) with Eq. (4).

$$\begin{aligned} \frac{P_i}{R_iT_i}u_iA_i &= \frac{P_e}{R_eT_e}u_eA_e \\ \frac{P_eA_e}{P_iA_i} = \frac{u_iR_eT_e}{u_eR_iT_i} &= \frac{M_i\sqrt{\gamma_iR_eT_e}}{M_e\sqrt{\gamma_eR_iT_i}} \end{aligned} \tag{8}$$

The following equation is derived from Eqs. (8) and (6).

$$\left(1+\gamma_iM_i^2\right)+\tilde{F} = \left(1+\gamma_eM_e^2\right)\frac{M_i\sqrt{\gamma_iR_eT_e}}{M_e\sqrt{\gamma_eR_iT_i}} \tag{9}$$

Eq. (9) is the momentum equation and is represented in terms of the Mach number and temperature. From the energy equation of Eq. (3), speed $u$ can be replaced by Mach number $M$.

$$h_i + \frac{1}{2}\gamma_iR_iT_iM_i^2 = h_e + \frac{1}{2}\gamma_eR_eT_eM_e^2 \tag{10}$$

where $h_i$ and $h_e$ are the enthalpy per unit mass. For the mixture, the enthalpy can be computed with the following equation.

$$h(T) = \sum_{k=1}^{Ns} y_k h_k(T)$$

$$h_k(T) = \int_{T_0}^{T} C_{pk}(T)dT + h_k(T_0)$$

Here, $y_k$ is the mass fraction of chemical species $k$, and $Ns$ is the number of chemical species. Enthalpy $h_k$ for species $k$ at temperature $T$ can be defined as the integration of constant pressure specific heat $C_{pk}$. Here, $T_0$ is the reference temperature of enthalpy (generally 298.15 K), and $h_k(T_0)$ is the heat of formation at $T_0$. Finally, the enthalpy of mixture can be expressed as

$$h(T) = \sum_{k=1}^{Ns}\left(y_k\int_{T_0}^{T} C_{pk}(T)dT\right) + h^0(T_0)$$

$$h^0(T_0) = \sum_{k=1}^{Ns} y_k h_k(T_0)$$

Here, $h^0(T_0)$ is the heat of formation for the mixture. This equation requires $C_{pk}(T)$ which is generally represented as high order polynomial of temperature; evaluation of enthalpy requires many computations. Moreover, numerical iteration is required to get temperature from the enthalpy. If the specific heat is averaged properly, it can be treated as constant. In this case, the analysis can become very simple. The energy equation becomes as follows:

$$h(T) = \bar{C}_p(T-T_0) + h^0(T_0)\,,\ \bar{C}_p = \sum_{k=1}^{Ns} y_k\bar{C}_{pk}$$

Here, $\bar{C}_{pk}$ is the averaged specific heat for species $k$, and $\bar{C}_p$

Table 1. Summary of S225 experiment setup

| | |
|---|---|
| Premixed Combustible Gas | $2H_2+O_2+5CO_2$ |
| Pressure ($P_1$) | 40 bar |
| Temperature ($T_1$) | 300 K |
| Speed of Sound ($a$) | 320.9 m/s |
| Launch Speed of Projectile ($u_0$) | 1800 m/s |
| Launch Mach Number of Projectile ($M_0$) | 5.609 |
| C-J Detonation Speed ($D$) | 1316.8 m/s |
| Over-driven Factor ($u_0/D$) | 1.367 |
| Caliber of Accelerator Tube ($d_1$) | 42 mm (approximately) |
| Diameter of Projectile ($d_p$) | 30 mm |
| Mass of Projectile (m) | 130 g |
| Cross-sectional Area of Accelerator Tube ($A_1=\pi d_1^2/4$) | 1381 mm$^2$ |
| Cross-sectional Area of Projectile ($A_p=\pi d_p^2/4$) | 706.86 mm$^2$ |
| Cross-sectional Area of Combustor ($A_2=A_3=A_1-A_p$) | 674.14 mm$^2$ |
| Inlet Area Ratio ($A_2/A_1$) | 0.4881 |
| Nozzle Area Ratio ($A_1/A_3$) | 2.0364 |
| Length of Accelerator Tube ($S$) | 4.8 m |

DOI: http://dx.doi.org/10.5139/IJASS.2016.17.3.358

is the averaged specific heat of mixture. The simplest method to obtain the averaged specific heat $\bar{C}_{pk}$ is arithmetic mean of $C_{pk}(T_0)$ and $C_{pk}(T)$; it is very easy method but does not exactly satisfy $h(T)$. The next method is enthalpy based average as following equation.

$$\bar{C}_{pk} = \frac{h_k(T) - h_k(T_0)}{T - T_0} = \frac{\int_{T_0}^{T} C_{pk}(T)dT}{T - T_0}$$

This method exactly satisfies enthalpy if the two temperature $T$ and $T_0$ are properly selected; however, generally $T$ is unknown value. If specific heat can be represented as constant, specific heat ratio $r$ and gas constant $R$ are also can be represented as constant. In this case, the momentum equation of Eq. (9) and energy equation of Eq. (10) can be simplified.

$$(1+\gamma M_i^2) + \tilde{F} = (1+\gamma M_e^2)\frac{M_i}{M_e}\sqrt{\frac{T_e}{T_i}} \tag{11}$$

$$\bar{C}_p T_i + \frac{1}{2}\gamma R T_i M_i^2 + q = \bar{C}_p T_e + \frac{1}{2}\gamma R T_e M_e^2 \tag{12}$$

Here, $q = h_i^0(T_0) - h_e^0(T_0)$ is the heat release, which is the difference in the enthalpy of formation between the two states. From the definitions of the specific heat and specific heat ratio, the specific heat can be represented with the specific heat ratio $r$ and gas constant $R$.

$$\bar{C}_p = \frac{\gamma}{\gamma - 1}R$$

Eq. (12) can be simplified by using the previous relation.

$$1 + \frac{\gamma-1}{2}M_i^2 + \tilde{q} = \frac{T_e}{T_i}\left(1 + \frac{\gamma-1}{2}M_e^2\right) \tag{13}$$

Here, $\tilde{q} = \dfrac{q}{\bar{C}_p T_i}$ is the non-dimensional heat release. The temperature ratio between the two states is

$$\frac{T_e}{T_i} = \frac{1 + \frac{\gamma-1}{2}M_i^2 + \tilde{q}}{1 + \frac{\gamma-1}{2}M_e^2} \tag{14}$$

When the process is isentropic, $q$ and $\tilde{q}$ are zero (adiabatic). The following isentropic relation can then be applied.

$$\left(\frac{P_e}{P_i}\right)^{\frac{\gamma-1}{\gamma}} = \left(\frac{\rho_e}{\rho_i}\right)^{\gamma-1} = \frac{T_e}{T_i}$$

The temperature, pressure, and density can be represented as a function of the Mach number in an isentropic process:

$$\frac{T_e}{T_i} = \frac{1 + \frac{\gamma-1}{2}M_i^2}{1 + \frac{\gamma-1}{2}M_e^2} \tag{15}$$

$$\frac{P_e}{P_i} = \left(\frac{T_e}{T_i}\right)^{\frac{\gamma}{\gamma-1}} = \left(\frac{1 + \frac{\gamma-1}{2}M_i^2}{1 + \frac{\gamma-1}{2}M_e^2}\right)^{\frac{\gamma}{\gamma-1}} \tag{16}$$

$$\frac{\rho_e}{\rho_i} = \left(\frac{T_e}{T_i}\right)^{\frac{1}{\gamma-1}} = \left(\frac{1 + \frac{\gamma-1}{2}M_i^2}{1 + \frac{\gamma-1}{2}M_e^2}\right)^{\frac{1}{\gamma-1}} \tag{17}$$

From the continuum equation of Eq. (1), the area ratio between two points can be derived.

$$\frac{A_e}{A_i} = \frac{\rho_i u_i}{\rho_e u_e} = \frac{\rho_i M_i \sqrt{\gamma R T_i}}{\rho_e M_e \sqrt{\gamma R T_e}} = \frac{\rho_i M_i \sqrt{T_i}}{\rho_e M_e \sqrt{T_e}} \tag{18}$$

The solution procedures are very simple in isentropic processes; if the inflow state and area ratio $A_e/A_i$ are known, the outflow Mach number can be computed using Eq. (18), and the other properties can be derived from Eqs. (15)-(17).

## 3. Theoretical Analysis for Each Example

Figure 3 shows the schematic of the theoretical analysis following the S225 experiment, and table 2 summarizes the assumptions for each case. The flow field is supersonic for

Table 2. Examples for theoretical analysis; expansion in nozzle was regarded as isentropic for all cases.

| Case | $C_p$, $\gamma$ | Assumption at the inlet | Combustible mixture | Averaged acceleration | Final speed |
|---|---|---|---|---|---|
| 1 | $C_p = \bar{C}_p$, $\gamma = 1.4$ | Isentropic compression | $2H_2+O_2+5CO_2$ | 21203.6 G | 2288 m/s |
| 2 | | Isentropic compression with shock wave drag | | 16125.9 G | 2181 m/s |
| 3 | | Shock wave compression | | 18916.8 G | 2240 m/s |
| 4 | $C_p(T)$, $\gamma(T)$ | Shock wave compression | $2H_2+O_2+5CO_2$ | 11625.3 G | 2082 m/s |
| 5 | | | $2H_2+O_2+5CO_2+0.3Al$ | 16078.4 G | 2180 m/s |
| 6 | | | $2H_2+O_2+5CO_2+0.15Al$ | 13811.4 G | 2131 m/s |
| 7 | | | $2H_2+O_2+5CO_2+0.15Al$ | 12413.8 G | 2099 m/s |

the ram accelerator in superdetonative mode; the analysis should be performed step-by-step from the inlet to the nozzle.

The drag acts on the inlet, and the thrust is generated at nozzle. After the drag and thrust are obtained, the net thrust and acceleration can be computed. The speed was computed assuming constant acceleration except in case 7. In this case, the increasing inflow speed due to the acceleration of the projectile was considered; the acceleration was computed for increments of 0.1 from Mach number 5.6 to 7.0, and each acceleration was adopted as the projectile accelerated.

### 3.1 Assumptions for specific heat and specific heat ratio

The specific heat dramatically increases as the temperature increases. If the temperature variation is large, the specific heat should be treated as a function of the temperature. In order to consider the temperature-dependent specific heat, the NASA Glenn coefficient for constant pressure specific heat was used [6]. The specific heat ratio was computed from its definition: $\gamma = C_p(T)/C_v(T)$.

If the specific heat can be treated as constant, the analysis becomes very simple. In this research, the averaged specific heat was obtained from the arithmetic mean of the specific heat at two temperatures: 300 K (temperature before combustion) and 2500 K (approximate temperature after combustion). The specific heat ratio followed that of the cold diatomic of gases ($\gamma = 1.4$).

In cases 4–7, the specific heat was evaluated as function of temperature, and the momentum equation of Eq. (9) and energy equation of Eq. (10) were used. In cases 1–3, the specific heat was assumed to be constant, and the momentum equation of Eq. (11) and energy equation of Eq. (14) were used.

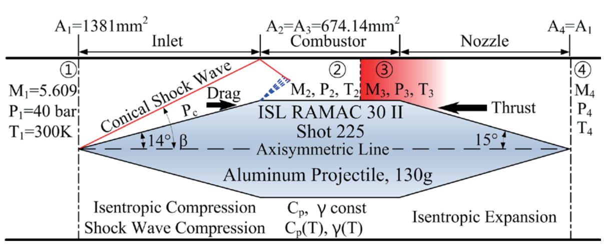


Fig. 3. Schematic of theoretical analysis

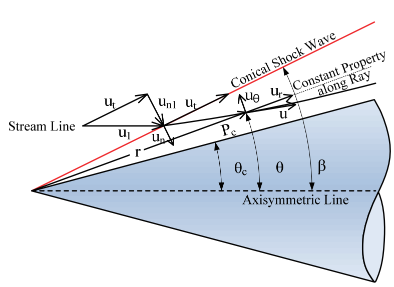


Fig. 4. Schematic of conical shock wave. The normal and tangential speeds to the shock wave are $u_{n1}$ and $u_t$, respectively. The speeds along the layer and normal to the layer are $u_r$ and $u_\theta$, respectively.

### 3.2 Assumptions for compression at inlet

The property behind the inlet is the input condition of combustor. A conical shock wave is generated on the cone in the supersonic flow field, and the pressure on the cone generates the drag. Therefore, both the property behind the inlet and the drag should be predicted.

For rigorous analysis, the drag should be predicted properly, and all of the conservation equations should be satisfied; the drag can be estimated from the Taylor-Maccoll equation [7], and the flow property can be computed from the conservation equations. The rigorous approach was adopted for cases 3-7.

In order to evaluate the exact drag, the pressure on the cone surface is required. The downstream flow solution of the conical shock wave can be obtained from the following Taylor-Maccoll equation [7]:

$$\frac{\gamma-1}{2}\left[u_{\max}{}^2 - u_r{}^2 - \left(\frac{du_r}{d\theta}\right)^2\right]\left[2u_r + \frac{du_r}{d\theta}\cot\theta + \frac{d^2u_r}{d\theta^2}\right]$$
$$-\frac{du_r}{d\theta}\left[u_r\frac{du_r}{d\theta} + \frac{du_r}{d\theta}\frac{d^2u_r}{d\theta^2}\right] = 0$$

where $u_{\max} = h + u^2/2$

The Taylor-Maccoll equation is an ordinary differential equation and should be solved with a numerical method (e.g., Runge-Kutta method). The speed just behind the shock wave is required for the initial condition of the Taylor-Maccoll equation. The normal Mach number $M_n$, pressure $P_s$, and temperature $T_s$ behind the shock wave can be obtained from the normal shock wave relation:

$$M_n{}^2 = \frac{M_{n1}{}^2 + \dfrac{2}{\gamma-1}}{\dfrac{2\gamma}{\gamma-1}M_{n1}{}^2 - 1}$$

$$\frac{P_s}{P_1} = 1 + \frac{2\gamma}{\gamma+1}\left(M_{n1}{}^2 - 1\right)$$

$$\frac{T_s}{T_1} = \left[1 + \frac{2\gamma}{\gamma+1}\left(M_{n1}{}^2 - 1\right)\right]\left[\frac{2+(\gamma-1)M_{n1}{}^2}{(\gamma+1)M_{n1}{}^2}\right]$$

The tangential speed $u_t$ is preserved across the shock wave, and the normal speed behind the shock wave $u_n$ can be computed from the definition of the Mach number: $u_n = M_n\sqrt{\gamma R T_s}$

DOI: http://dx.doi.org/10.5139/IJASS.2016.17.3.358

The speed just behind the shock wave can be determined from $u_n$ and $u_t$. If the initial condition is obtained, the Taylor–Maccoll equation can be integrated from shock wave $\theta=\beta$ to cone surface $\theta=\theta_c$. The semi-vertex angle of cone $\theta_c$ can be determined when the normal speed to the ray is zero ($u_0=0$). If shock wave angle $\beta$ is assumed, $\theta_c$ is determined; the iterative method is required in order to obtain the desired $\theta_c$. After the speed or Mach number behind the shock wave is obtained, other properties like the pressure or temperature can be determined from the isentropic relation; the flow field behind the shock wave is isentropic. If the pressure on the cone $P_c$ is obtained, the drag can be obtained from $F=P_cA_p$. When the conical shock wave was solved for the inflow condition of S225 ($M_1$, $P_1$, $T_1$, $\gamma$ = 1.4), for example, the pressure on the cone $P_c$ and drag $F$ were determined as 157.75 bar and 11150.5 N, respectively.

If the temperature-dependent specific heat is considered, the property behind the inlet can be determined by solving the momentum and energy equations of Eqs. (9) and (10), respectively:

$$\left(1+\gamma_1 M_1^2\right)+\tilde{F}=\left(1+\gamma_2 M_2^2\right)\frac{M_1\sqrt{\gamma_1 R_2 T_2}}{M_2\sqrt{\gamma_2 R_1 T_1}}$$

$$h_1+\frac{1}{2}\gamma_1 R_1 T_1 M_1^2=h_2+\frac{1}{2}\gamma_2 R_2 T_2 M_2^2$$

If the specific heat is assumed to be constant, the momentum and energy equations are Eqs. (11) and (14).

$$\left(1+\gamma M_1^2\right)+\tilde{F}=\left(1+\gamma M_2^2\right)\frac{M_1}{M_2}\sqrt{\frac{T_2}{T_1}}$$

$$\frac{T_2}{T_1}=\frac{1+\frac{\gamma-1}{2}M_1^2}{1+\frac{\gamma-1}{2}M_2^2}$$

After $M_2$ and $T_2$ are obtained, $P_2$ can be obtained from Eq. (7).

The conical shock wave can be approximated with the isentropic compression wave in order to simplify the analysis. However, the isentropic assumption does not consider the total pressure loss by the shock wave. Therefore, such an approximation may cause an error in the estimated drag and output properties. The simplified approach was used for cases 1 and 2.

If the compression in the inlet is approximated with the isentropic process, $M_2$ can be obtained from the area ratio of Eq. (18). After $M_2$ is obtained, other properties (e.g., $P_2$ and $T_2$) can be obtained using Eqs. (15) and (16).

$$\frac{A_2}{A_1}=\frac{M_1}{M_2}\left(\frac{1+\frac{\gamma-1}{2}M_2^2}{1+\frac{\gamma-1}{2}M_1^2}\right)^{\frac{\gamma+1}{2(\gamma-1)}}$$

$$\frac{T_2}{T_1}=\frac{1+\frac{\gamma-1}{2}M_1^2}{1+\frac{\gamma-1}{2}M_2^2}$$

$$\frac{P_2}{P_1}=\left(\frac{1+\frac{\gamma-1}{2}M_1^2}{1+\frac{\gamma-1}{2}M_2^2}\right)^{\frac{\gamma}{\gamma-1}}$$

The drag can be obtained from Eq. (6):

$$\tilde{F}=\left(1+\gamma M_2^2\right)\frac{P_2 A_2}{P_1 A_1}-\left(1+\gamma M_1^2\right)$$

A drag of $F$ = -4679.16 N was obtained under the assumption of isentropic compression for $M_1$, $P_1$, $T_1$, $\gamma$ = 1.4, and $A_2/A_1 = 0.4881$.

Case 1 used the isentropic assumption in the inlet. Case 2 used the properties of isentropic assumption excluding the drag; the drag followed the same properties as those for shock wave compression.

### 3.3 Assumptions for combustion

The premixed combustible gas for S225 was $2H_2 + O_2 + 5CO_2$: the stoichiometric mixture of $H_2$ and $O_2$ was diluted with $5CO_2$. If complete combustion is assumed, the reaction formula is $2H_2 + O_2 + 5CO_2 \rightarrow 2H_2O + 5CO_2$. In

Table 3. Specific heat at 300 and 2500 K and averaged specific heat [J/mol•K]

| Chemical Species | Specific Heat at 300 K | Specific Heat at 2500 K | Average |
|---|---|---|---|
| $H_2O$ | 33.596 | 54.777 | 44.187 |
| $CO_2$ | 37.220 | 61.443 | 49.332 |
| $2H_2O+5CO_2$ | 36.185 | 59.538 | 47.862 |

Table 4. Heat release of each reaction

| Mixture | Heat Release [J/mol] | Increasing Ratio |
|---|---|---|
| $2H_2+O_2+5CO_2$ | 60456 | - |
| $2H_2+O_2+5CO_2+0.15Al$ | 66952 | 10.7% |
| $2H_2+O_2+5CO_2+0.3Al$ | 73212 | 21.2% |

this case, the products are independent of the final pressure and temperature. However, dissociation occurs at high temperatures; the combustion products are determined by the conditions that minimize the Gibbs free energy (i.e., equilibrium state). In order to investigate the effect of chemical equilibrium, the constant pressure combustion for $2H_2 + O_2 + 5CO_2$ at 40 bar and 300 K was computed using CEA2 [8], which can compute equilibrium combustion chemistry. The major products of the equilibrium reaction were $H_2O$ and $CO_2$; the other species were very minor. If combustion of aluminum was considered, additional oxygen was required for aluminum oxidation. When the equilibrium reaction with aluminum was computed using CEA2, the major products of the equilibrium reaction were $H_2O$, $Al_2O_3$, $CO_2$, and CO; additional oxygen for the reaction with aluminum was supplied from the dissociation of $CO_2$. As a result, the chemical reaction can be generalized by the following formula:

$$2H_2 + O_2 + 5CO_2 + x\mathrm{Al}$$
$$\rightarrow 2H_2O + \frac{x}{2}Al_2O_3 + \left(5\text{-}\frac{3x}{2}\right)CO_2 + \frac{3x}{2}CO$$

When aluminum is not included ($x$ = 0), the formula represents the complete combustion of $2H_2 + O_2 + 5CO_2$. If the combustion is affected by aluminum, the acceleration can be increased. Two representative case $2H_2 + O_2 + 5CO_2 + 0.15Al$ and $2H_2 + O_2 + 5CO_2 + 0.3Al$ were selected from repeated calculation for various mixtures; the former showed the best fit for the overall speed trajectory, the latter resembled in the maximum acceleration in the experiment. Table 3 summarizes the heat releases of the reactions.

### 3.4 Assumptions at nozzle

The product of the combustion expands at the nozzle to generate thrust. In superdetonative mode, the flow field of the ram accelerator is supersonic. The expansion in supersonic flow can be regarded as isentropic. The exit Mach number can be obtained from the area ratio of Eq. (18), and the other properties can be obtained from Eqs. (15)-(17). The thrust can be computed by using Eq. (6).

## 4. Discussion on Theoretical Analysis

Table 2 and Fig. 5 summarize the theoretical analysis results. Case 1, which used isentropic compression at the inlet, showed the highest acceleration. Case 2, which also considered the drag of the shock wave, showed decreased acceleration relative to case 1.

Case 2 showed the same results as the theoretical analysis from ISL [5]. The results also matched the experimental results well. However, case 3, which considered shock wave compression, showed a very different result. In case 3, the pressure behind the shock wave and in the combustor was higher than that of the isentropic compression. Thus, shock wave compression might generate more thrust at the nozzle. However, the loss due to the shock wave severely decreases the net thrust. As a result, shock wave compression (case 3) produced less acceleration than isentropic compression (case 1). Case 2 followed the flow property of case 1 and drag of case 3. Thus, case 2 underestimated the pressure and

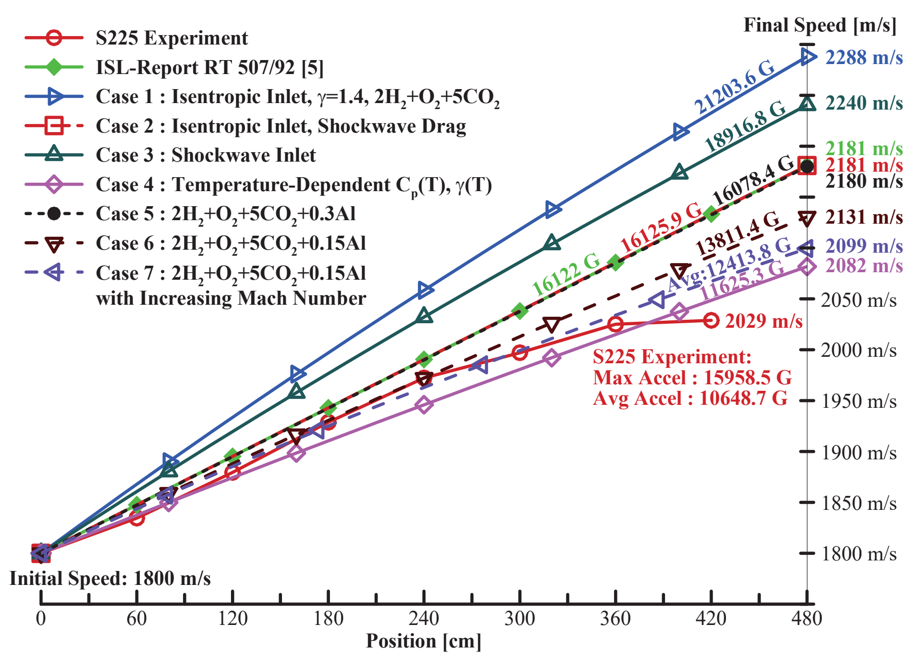


Fig. 5. Speed and acceleration for theoretical analysis

thrust compared to case 3.

Whereas case 3 showed a higher acceleration than the experimental results, case 4, which considered the temperature-dependent specific heat, showed a lower acceleration. The averaged specific heat, which is the arithmetic mean of the specific heat, was 47.86 J/mol·K in case 3. In case 4, the averaged specific heat was approximately 50 J/mol·K; this was computed from the enthalpy base specific heat of $(h_3-h_2)/(T_3-T_2)$. Because the specific heat was underestimated in case 3, the temperature increment was overestimated. The specific heat ratio in case 3, was 1.4 which followed that of the cold diatomic gases. In contrast, case 4 used the temperature-dependent specific heat ratio for each chemical species; the specific heat ratio was 1.32 for the inflow condition and was lower than 1.2 after combustion. The flow property was sensitive to variation in the specific heat ratio; generally, the pressure or temperature ratio depends on $\gamma$-1 rather than $\gamma$, as in Eq. (15) or (16). Thus, the exact specific heat should be considered in order to obtain the exact flow property.

Cases 5 and 6 considered the additional energy due to the combustion of aluminum. When the reaction was $2H_2$ + $O_2$ + $5CO_2$ + 0.3Al, the acceleration was comparable to the maximum acceleration of the experiment in Fig. 5. When the reaction was $2H_2$ + $O_2$ + $5CO_2$ + 0.15Al, the acceleration behavior before the projectile arrived at 240 cm position quietly agreed with the experimental result.

Case 7 considered an increasing inflow speed due to the acceleration of the projectile and showed a lower speed than case 6 because the drag increased with the speed; the acceleration decreased by approximately 11%. And, we can easily recognize that this case showed the best fitting with the experimental result S225. There is still some deviation after the flight distance 360 cm; significant ablation of projectile would cause unstable flight problem in the experiment.

## 5. Conclusion

The theoretical analysis from ISL, which derived on the assumptions of isentropic compression and averaged specific heat, showed that the S225 experiment would not be affected by the heat of the aluminum reaction. However, present analysis showed a different result. The increment of heat due to aluminum combustion was approximately 11%, and the maximum effect might be 21%; further heat due to the combustion of aluminum may be available because the theoretical analysis in that investigation assumed inviscid flow.

Assumptions such as applying the isentropic process to the shock wave or a constant specific heat can simplify the analysis. Simplified analysis is frequently adopted for theoretical analysis because it can supply fast solutions. In this research, a rigorous analysis that satisfies the conservation law with temperature-dependent specific heat was suggested. Based on the fully rigorous analysis, the increase in heat due to the combustion of aluminum in the S225 experiment was properly understood; it was confirmed that aluminum combustion had influenced to the ram accelerator in superdetonative mode operation.

## Acknowledgement

This study is an international collaboration work between Seoul National University and the French-German Research Institute of Saint-Louis (ISL). The experiment had been solely performed by ISL. This work was partly supported by the BK 21 Plus and Space Technology Development Program through the National Research Foundation of Korea (NRF) grant funded by the Korea government (MSIP) (NRF-2015M1A3A3A02014343).

## References

[1] Hertzberg, A., Bruckner, A. P. and Bogdanoff, D. W., “Ram Accelerator: A New Chemical Method for Accelerating Projectiles to Ultrahigh Velocities”, *AIAA Journal*, Vol. 26, No. 2, 1988, pp. 195-203. DOI:10.2514/3.9872

[2] Bogdanoff, D. W., “Ram Accelerator Direct Space Launch System: New Concepts”, *Journal of Propulsion and Power*, Vol. 8, No. 2, 1992, pp. 481-490. DOI:10.2514/3.23502

[3] Seiler, F., Patz, G., Smeets, G. and Srulijes, J., “Influence of Projectile Material and Gas Composition on Superdetonative Combustion in ISL'S RAMAC 30”, *34th AIAA/ASME/SAE/ASEE Joint Propulsion Conference and Exhibit*, Cleveland, OH, July 13-15, 1998.

[4] Seiler, F., Patz, G., Smeets, G. and Srulijes, J., “Progress of Ram Acceleration with ISL's RAMAC30”, *Journal de Physique IV*, 10,PR11, 2000, Pr11-31.

[5] Smeets, G., Gatau, F. and Srulijes, J., “Rechenprogramm für Abschätzungen zur Ram-Rohrbeschleinigung”, *ISL-Report RT* 507/92, 1992

[6] McBride, B. J., Zehe, M. J. and Gordon, S., “NASA Glenn Coefficients for Calculating Thermodynamic Properties of Individual Species”, NASA/TP-2002-211556, 2002.

[7] Anderson J. D., *Modern Compressible Flow: With Historical Perspective*, New York, McGaw-Hill, 1990.

[8] McBride, B. J. and Gordon, S., N*ASA Glenn Chemical Equilibrium Program CEA2*, NASA Glenn Research Center, Cleveland, OH, 2004.

http://www.grc.nasa.gov/www/CEAWeb